

## Supporting Information

### Bright, Stable, and Efficient Red Light-emitting Electrochemical Cells using Contorted Nanographenes

Elisa Fresta, Kevin Baumgärtner, Juan Cabanillas-Gonzalez, Michael Mastalerz and Rubén D. Costa\*

#### Preparation and characterization of thin films

**1** was synthesized as reported previously.<sup>1,2</sup> Absorption spectra were recorded with a Perkin Elmer Lambda 35 UV-Vis spectrometer. The emission spectra and photoluminescence quantum yields ( $\phi$ ) values were measured with a FS5 Spectrofluorometer with integrating sphere SC-30 (Edinburgh Instruments). Excited states lifetimes ( $\tau$ ) of fluorescence emission were obtained with a TCSPC module ( $\lambda_{\text{exc}}$  377.6 nm).

The average lifetime can be obtained by using the depicted formula:

$$R(t) = \sum_{i=1}^2 A_i e^{-t/\tau_i} \quad \text{where } A_i \text{ is constant. The average lifetime can be obtained with:}$$
$$\langle \tau \rangle = \frac{A_1 \tau_1^2 + A_2 \tau_2^2}{A_1 \tau_1 + A_2 \tau_2}$$

Photoluminescence measurements at temperatures ranging from 77 K to 425 K were performed upon enclosing the **1** films in a CFV-Optistat (Oxford Instruments) equipped with a temperature controller. Thin-films were photoexcited with a TEEM Photonics passive Q-switch Nd:YAG laser (405 nm, 300 ps pulse duration, 170 Hz, pulse energy < 1 mJ) mildly focused on the sample (fluence < 10 mJcm<sup>-2</sup>). The photoluminescence emitted by the samples was dispersed by a grating inside a spectrometer (SP2500, Acton Research) and spectrally recorded with a liquid N<sub>2</sub>-cooled back depleted CCD (Princeton Instruments). Long pass filters were employed to reject stray light from the photoexcitation beam into the spectrometer. Photoluminescence spectra were acquired 10 minutes after the sample reached the desired temperature in order to ensure complete sample thermalization.

Thin films were prepared onto cleaned quartz slides from a filtered solution of **1** (15 mg/mL in THF to achieve 70 nm thickness or 5 mg/mL to achieve 30 nm thickness) by spin-coating them at 800 rpm for 30 s, at 1500 rpm for 30 s and at 3000 rpm for an additional 10 s. AFM measurements were carried out with a Park XE150 instrument (Park Systems Corp., Suwon, South Korea), and the Gwyddion evaluation software.

## Device fabrication and characterization

ITO substrates were purchased from Naranjo Substrates with an ITO thickness of 130 nm. They were extensively cleaned using detergent, water, ethanol, and propan-2-ol as solvents in an ultrasonic bath (frequency 37-70 Hz) for 15 min each. Afterwards, the slides were dried with N<sub>2</sub> gas and put in an UV-ozone cleaner for 8 min and used directly as described in the main text. If PEDOT:PSS is used to increase reproducibility, the clean plates were coated with 70 nm PEDOT:PSS layers via spin coating. To this end, an aqueous solution of PEDOT:PSS was filtered and mixed with propan-2-ol in a ratio of 3:1. From this solution, 50  $\mu$ L were dropped onto the substrate at a rotation speed of 2000 rpm and spun for 60 s. The resulting layers were dried on a hotplate at 120 °C and stored under N<sub>2</sub>. Thick active layers (70 nm) were deposited from a 10 mg/mL THF solution of **1** combined with a ion-doped matrix consisting of **1**:TMPE:LiOTf 1:0.15:0.05 mass ratio. This was prepared using THF solutions of TMPE with M<sub>w</sub> 450,000 (20 mg/mL), and LiOTf (10 mg/ml) and spin coated at 800 rpm for 30 s, at 1500 rpm for 30 s and at 3000 rpm for an additional 10 s, resulting in 70 nm of active layer thickness. The thin active layers (30 nm) were achieved by employing a 5 mg/mL solution of **1**, following the same procedure as above. In all cases, after the deposition of the active layer the devices were dried under vacuum for 2 h and transferred to an inert atmosphere glovebox (<0.1 ppm O<sub>2</sub> and H<sub>2</sub>O, Angstrom Engineering). Finally, Aluminum cathodes (90 nm) were thermally evaporated onto the active layer using a shadow mask under high vacuum (<1 x 10<sup>-6</sup> mbar) in an Angstrom Covap evaporator integrated into the inert atmosphere glovebox. The device active area was of 10 mm<sup>2</sup>. The device statistics involve up to five different devices – *i.e.*, a total number of 20 pixels. Time dependence of luminance, voltage, and current was measured by applying constant and/or pulsed voltage and current by monitoring the desired parameters simultaneously by using Avantes spectrophotometer (Avaspec-ULS2048L-USB2) in conjunction with a calibrated integrated sphere Avasphere 30-Irrad and Botest OLT OLED Lifetime-Test System. Electroluminescence spectra were recorded using the above mentioned spectrophotometer. Electrochemical impedance spectroscopic assays (EIS) were carried out with a potentiostat/galvanostat (Metrohm  $\mu$ AutolabIII) equipped with a frequency response analyser module (FRA2). Measurements were performed at the applied voltage range from 0 to 5 V and fitted with the Nova software using the circuit model shown in Figure S9. The AC signal amplitude was set to 10 mV, modulated in a frequency range from 10 Hz to 1 MHz. The Nova 1.11 software was used to obtain the parameters from the equivalent circuit. With this

data at hand, the resistance of the intrinsic non-doped region ( $R_{LEC}$ ) was directly obtained. The film conductivity (S/m) is measured at 0 V with the following equation:  $\sigma=d/(AR_{LEC})$ , where  $d$  is the thickness of the layer,  $A$  is the area of the electrodes, and  $R_{LEC}$  is the resistance of the active layer. Dynamic EIS measurement were performed at the constant voltage of 3 V and fitted using the circuit model shown in Figure S20. Upon performing the fitting, the capacitance was replaced with a constant phase element (CPE), which is the equivalent electrical circuit component that models the behavior of an imperfect capacitor. This is assumed to be caused by non-uniform current density distribution and/or reaction rates along the electrode surface, usually caused by an inhomogeneous surface. [4,5] The CPE's impedance is defined as  $C=Q^{1/\alpha}R_{LEC}^{(1-\alpha)/\alpha}$ , and  $\alpha$  ( $0 \leq \alpha \leq 1$ ).  $Q$  corresponds to  $1/|Z|$  at  $\omega = 1$  rad/s, where  $Z$  is the impedance; it represents no direct meaningful physical value. However, the CPE acts as pure resistor for  $\alpha = 0$  and pure capacitor for  $\alpha = 1$ . The thickness of the doped regions is calculated taking into account that  $d_{EDL}C_{EDL}=dC_{geo}$ , where  $d_{EDL}$ =thickness of the doped regions,  $C_{EDL}$ =capacitance associated to the doped regions,  $d$ =device thickness and  $C_{geo}$ =geometric capacitance obtained by fitting the circuit at 0 V.[4]. The intensity of the internal electric field is then calculated with  $E=V/d_{EDL}$ , where  $V$  is the constant applied voltage and  $d_{EDL}$  the thickness of the doped regions. The temperature of the devices upon driving was recorded with a FLIR 430-sc thermal camera. The EQE is defined as  $EQE=b\phi/2n^2$ , where  $b$  is the recombination efficiency (equal to 1 for two ohmic contacts),  $\phi$  is the fraction of excitons that decay radiatively, and  $n$  is the refractive index of the glass substrate and is equal to 1.5 (the factor  $1/2n^2$  represent the light out-coupling of the device). As **1** can only presents fluorescence emission,  $\phi$  is equal to  $1/4$  of the PL efficiency, as, statistically,  $1/4$  of the electron-hole recombination produces singlets.

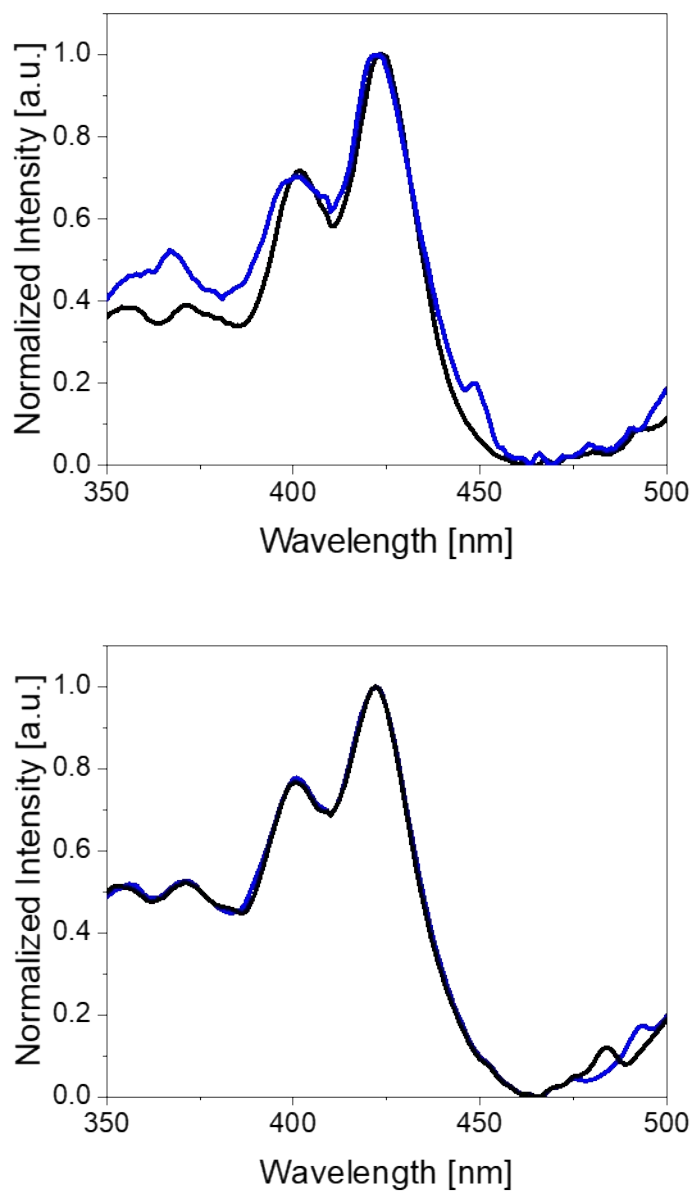


**Figure S1.** Excitation spectra at rt. of pristine **1** thin-film (top) and those used in devices with polyelectrolyte matrix (bottom) at  $\lambda_{em}$  of 598 nm (black) and 647 nm (blue).

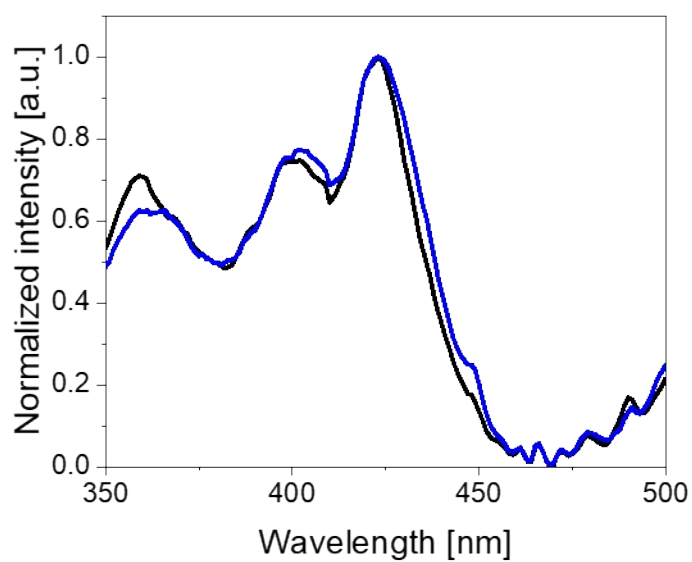
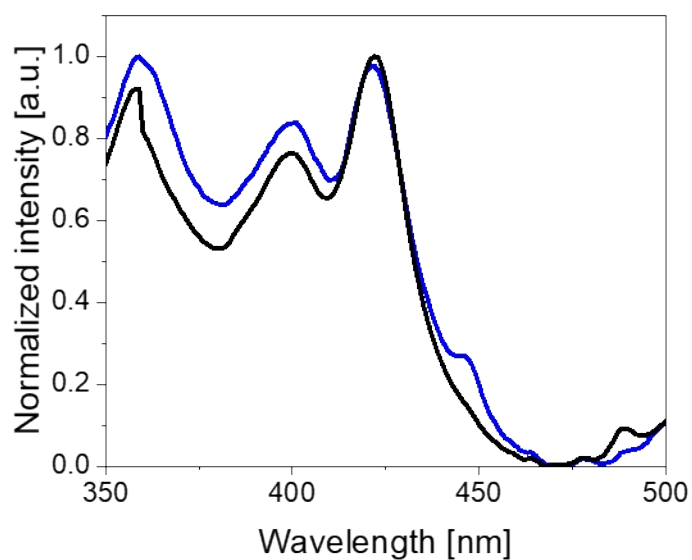


**Figure S2.** Excitation spectra at 77 K of pristine **1** thin-film (top) and those used in devices with polyelectrolyte matrix (bottom) at  $\lambda_{\text{em}}$  of 598 nm (black) and 647 nm (blue).

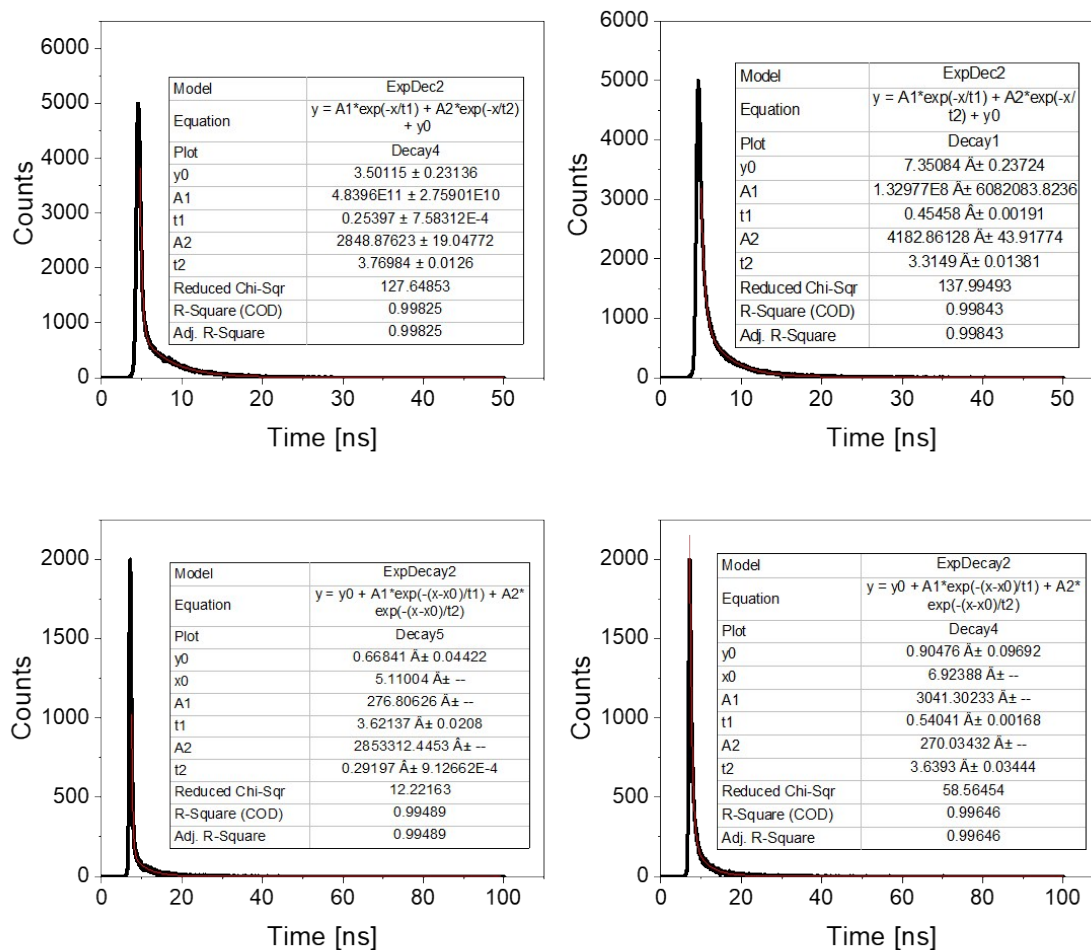


**Figure S3.** Excited-state decay profile ( $\lambda_{exc} = 377.6$  nm) measured at rt. of pristine **1** thin films pure (top) and those used in devices with polyelectrolyte matrix (bottom) at  $\lambda_{em}$  of 600 nm (left) and 650 nm (right). The exponential fittings are highlighted in red, while the parameters are gathered in the inset table.

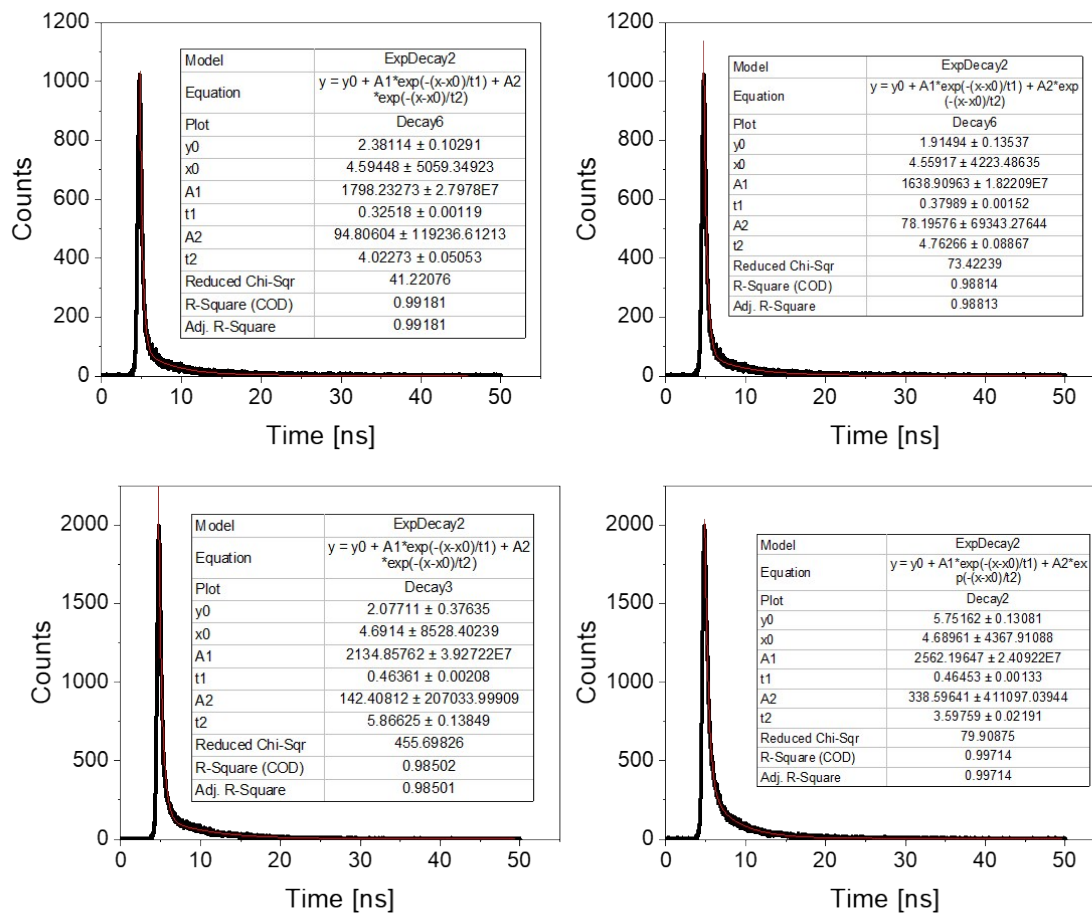


**Figure S4.** Excited-state decay profile ( $\lambda_{\text{exc}} = 377.6$  nm) measured at 77K of pristine **1** thin films pure (top) and those used in devices with polyelectrolyte matrix (bottom) at  $\lambda_{\text{em}}$  of 600 nm (left) and 650 nm (right). The exponential fittings are highlighted in red, while the parameters are gathered in the inset table.

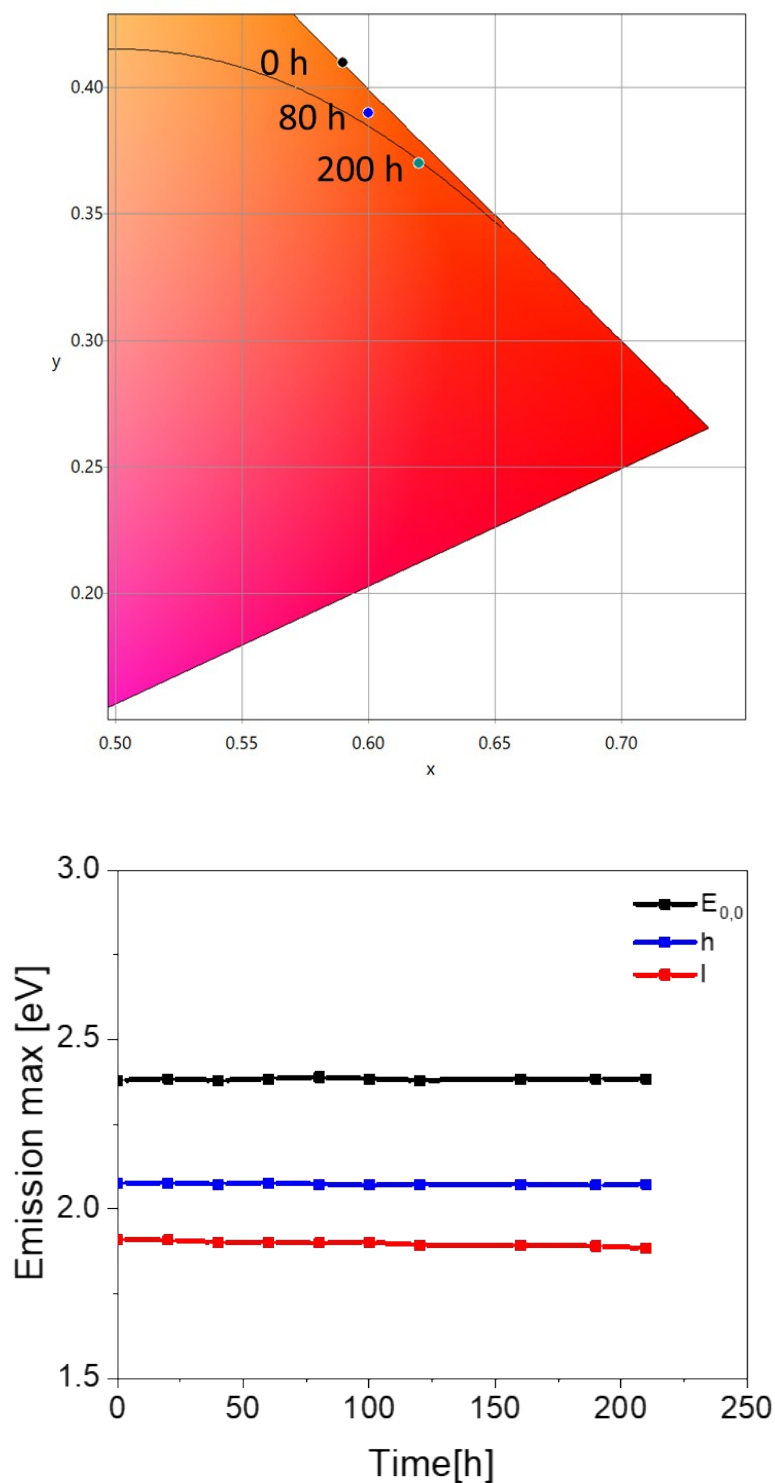


**Figure S5.** Top: Changes of the x/y CIE coordinates of **1** devices corresponding to the electroluminescence response of fresh (black), after 80 h (blue), and after 200 h (green) at a pulsed 25 mA current. Bottom: Changes in  $E_{0,0}$  band and emission wavelength maxima of h and l peaks (h=high energy, l=low energy) over time in **1** devices driven at a pulsed 25 mA current.

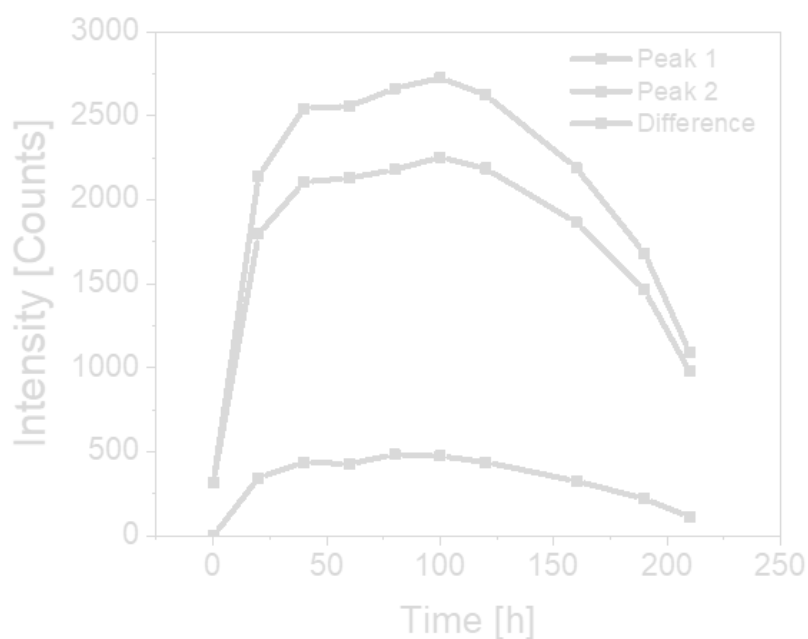


**Figure S6.** Changes of the intensity of the h and l peaks as well as their difference (h-l) over time (left) over time in **1** devices driven at a pulsed 25 mA current.

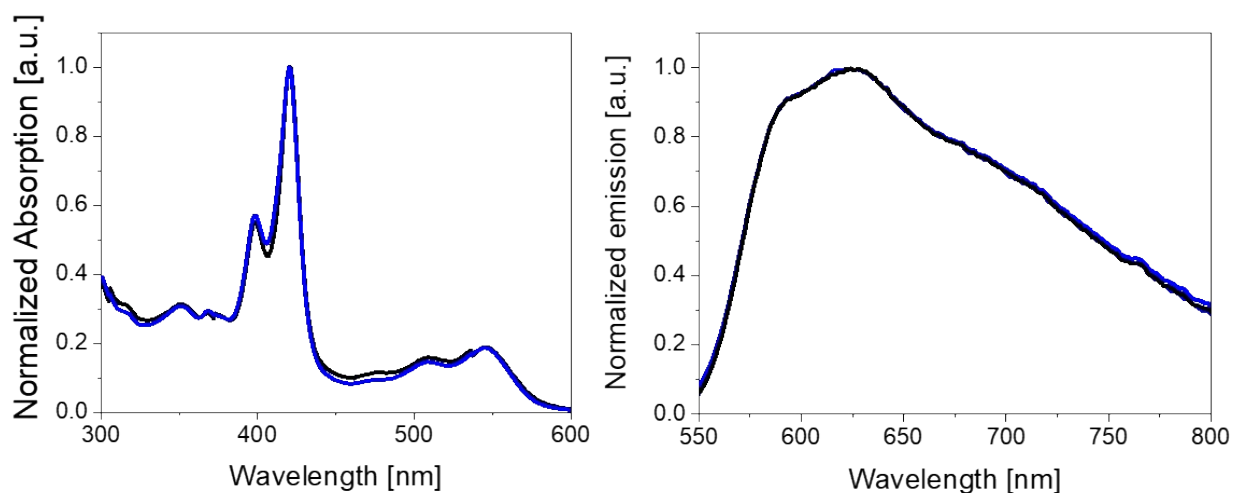


**Figure S7.** UV-Vis absorption (left) and emission (right) spectra of fresh (black) and used (blue) **1** devices.

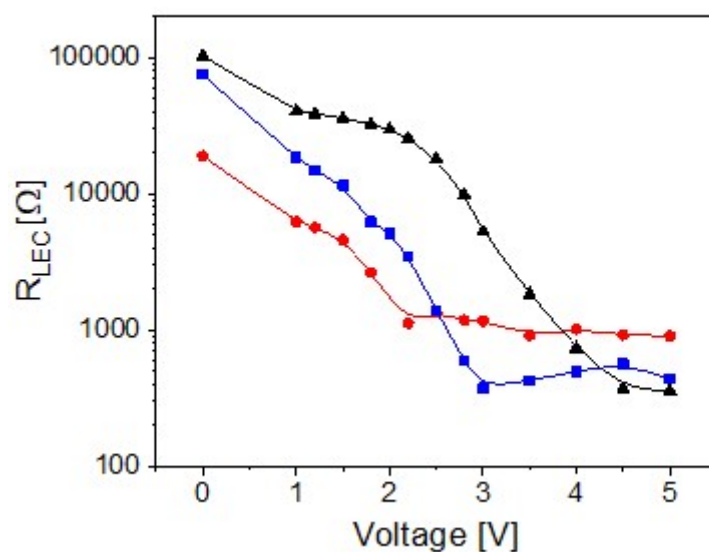


**Figure S8.** Static EIS assays applied to **1** devices to monitor the changes of the device behavior of fresh (black), used (red), and after heating at 60 °C (blue) devices with respect to resistance associated to the EDL and doped region formations upon increasing the applied voltage from 0 to 5 V.

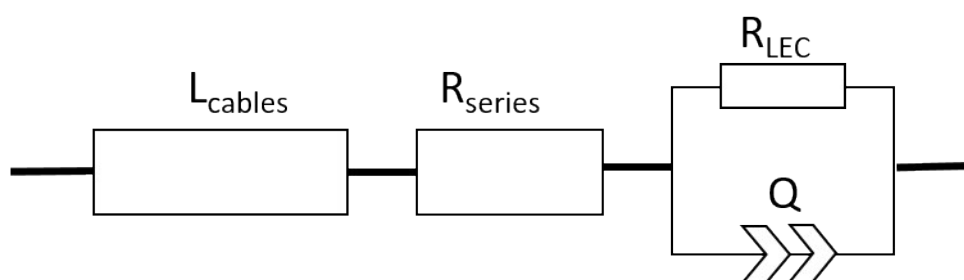


**Figure S9.** Simplified circuit model with electrical resistance ( $R_{LEC}$ ) and admittance  $Q$  used for static EIS assays. A series resistor ( $R_{series}$ ) and inductor elements for the cables ( $L_{cables}$ ) were also included.

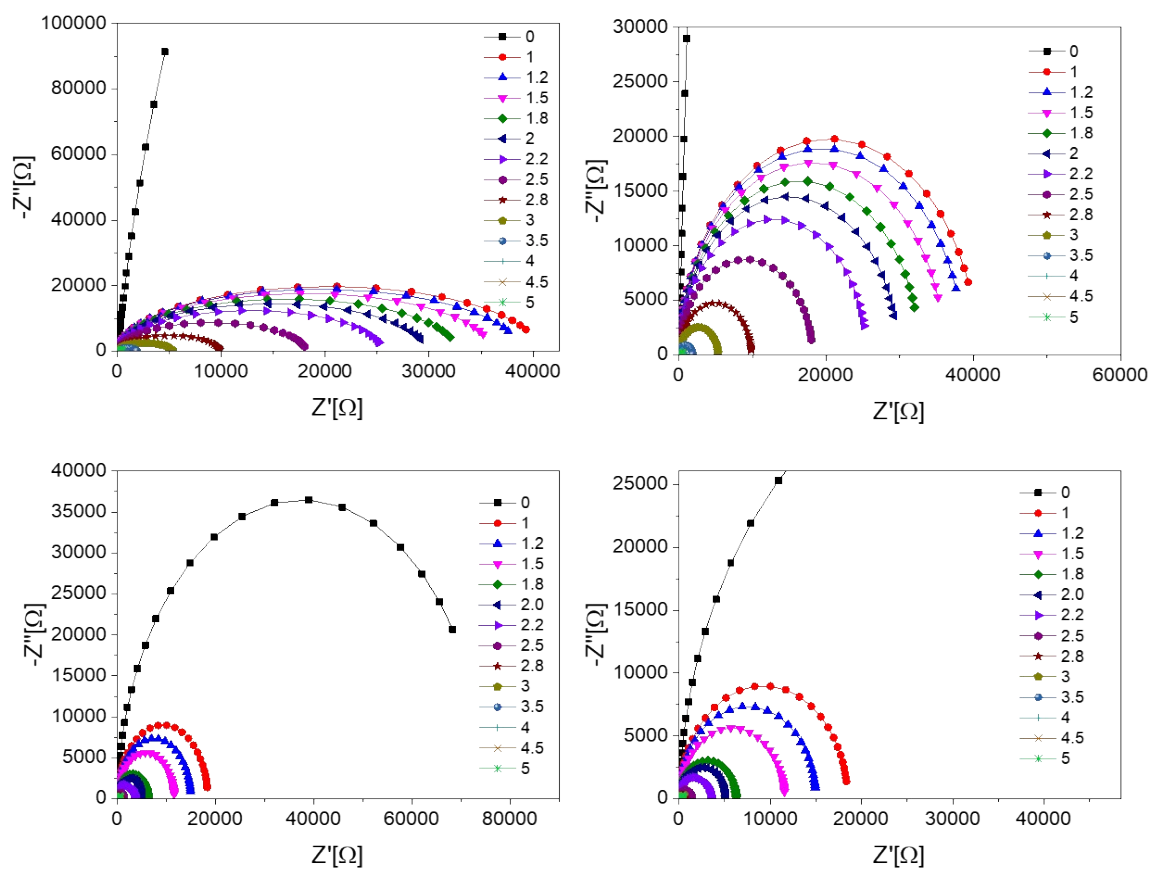


**Figure S10.** Nyquist plots of fresh (top left), with zoom into the 1-5 V region (top right), and used heated at  $60^\circ\text{C}$  (bottom left), with zoom into the 1-5 V region (bottom right), **1** devices measured upon constant bias (see legend). The fittings are shown in solid lines.

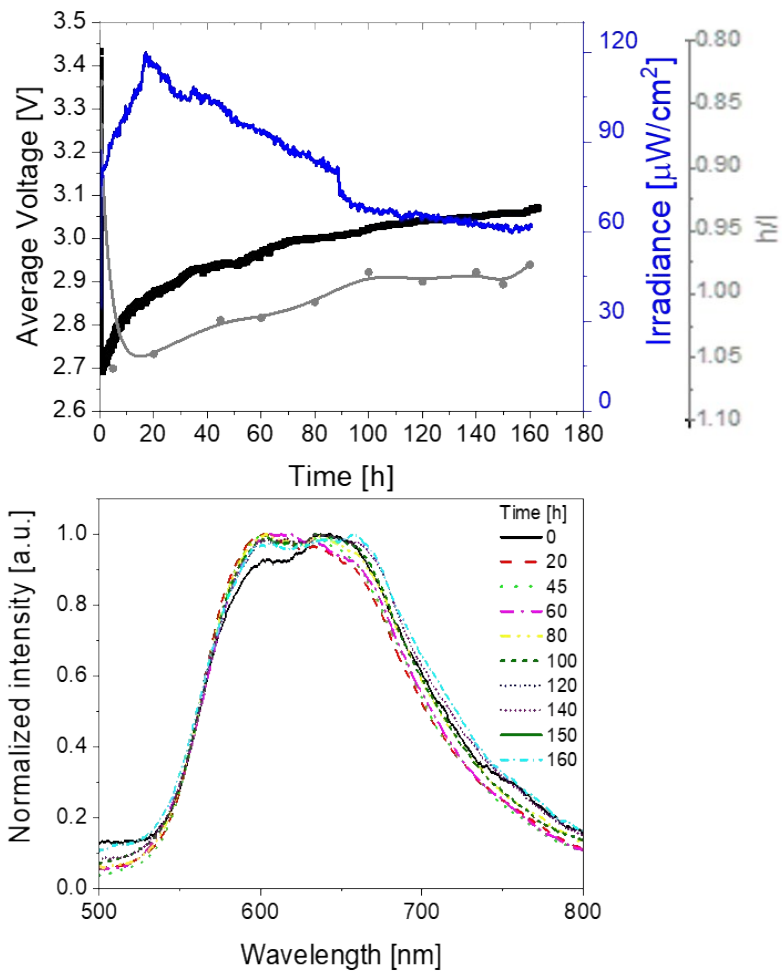


**Figure S11.** Average voltage, irradiance, and  $h/l$  ratio ( $h$ =high energy peak and  $l$ =low energy peak) (top), as well as electroluminescence spectra (bottom) over time (see legend) for used **1** devices driven at pulsed 25 mA current.

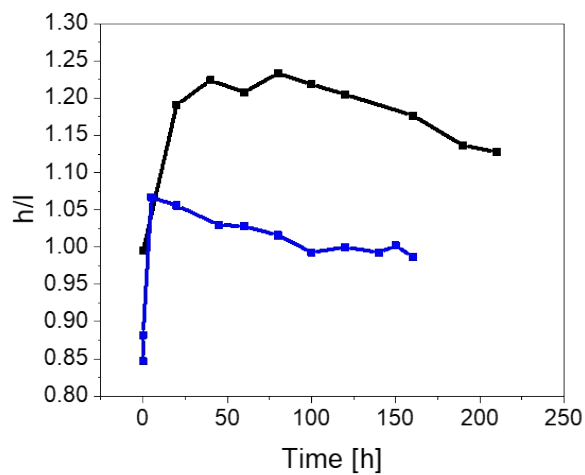


**Figure S12.** h/l (h=high energy peak and l=low energy peak) ratio over time for fresh (black) and used (blue) **1** devices run until lifetime at the pulsed current of 25 mA.

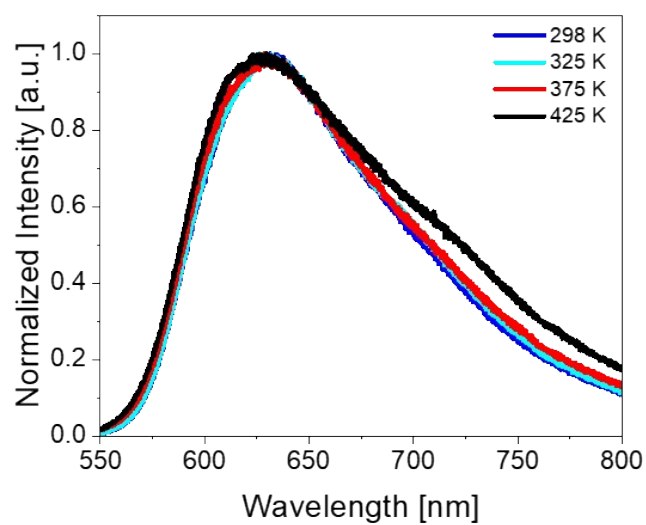
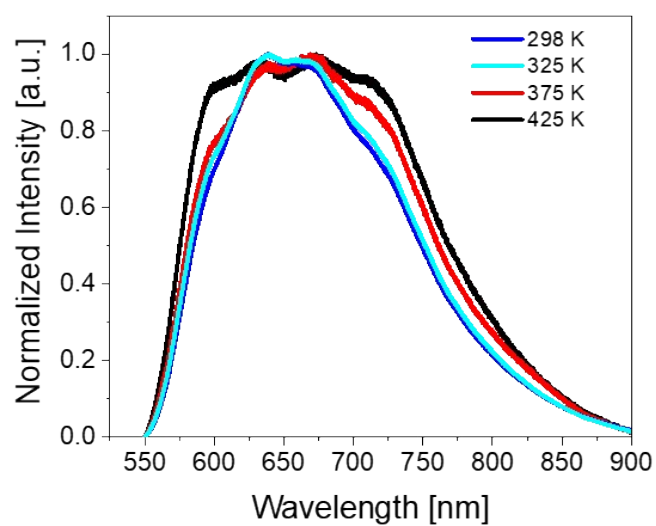
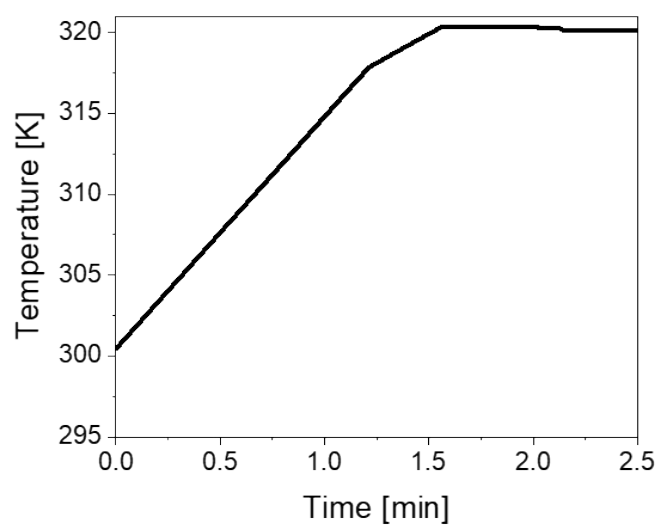


**Figure S13.** Top: Temperature rise of **1** device at 25 mA. Bottom: photoluminescence at different temperatures of pristine **1** thin films (center) and those used in devices with the ionic polyelectrolyte matrix (bottom). The films were prepared onto quartz slides.

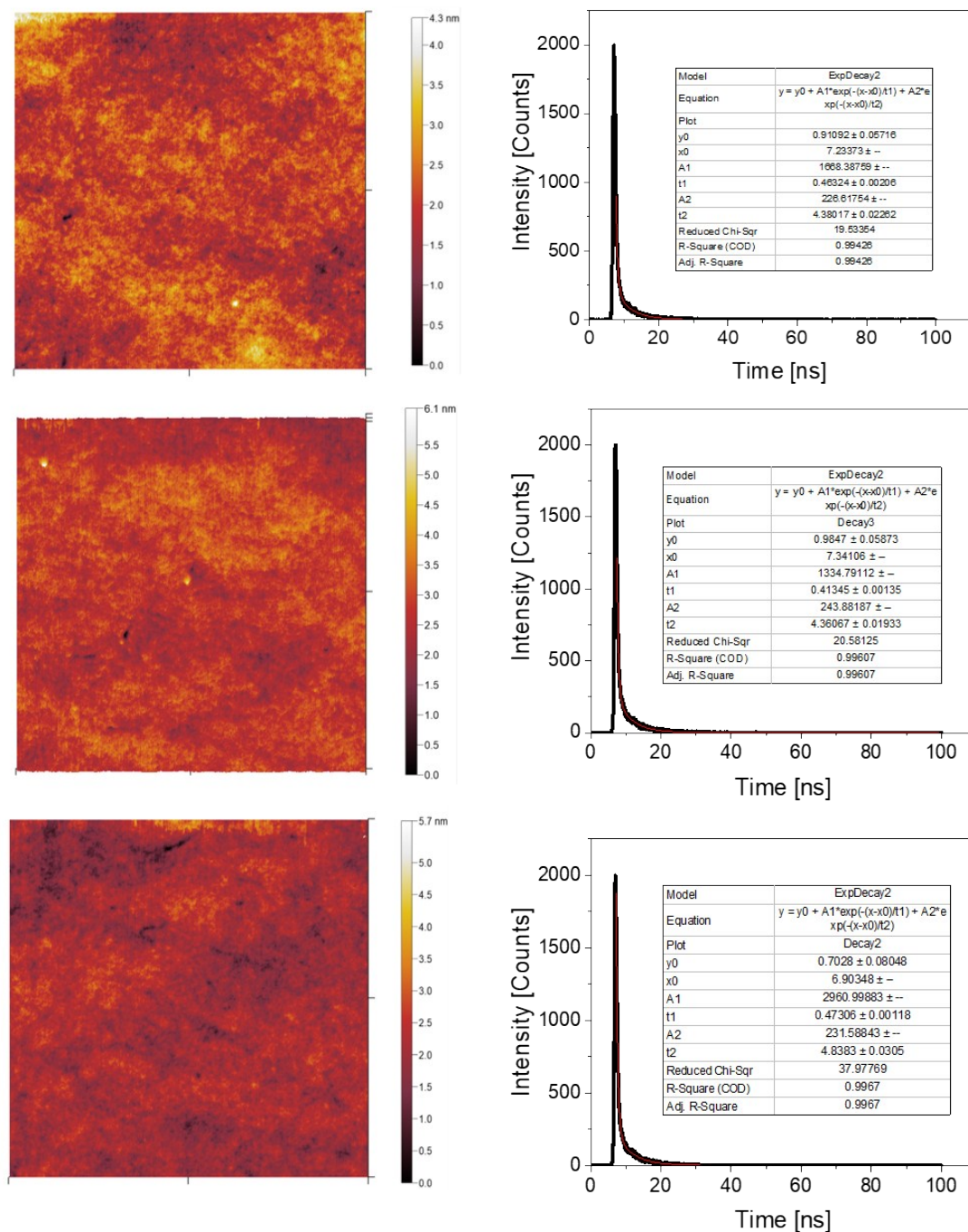


**Figure S14.** AFM measurements (left) and excited-state decay profile ( $\lambda_{\text{exc}} = 377.6 \text{ nm}$ ;  $\lambda_{\text{em}} = 600 \text{ nm}$ ) (right) of fresh **1** devices (top) and those kept at  $60^\circ\text{C}$  for 1 day (center) and for 10 days (bottom). The exponential fittings are highlighted in red and the parameter are gathered in the inset table.

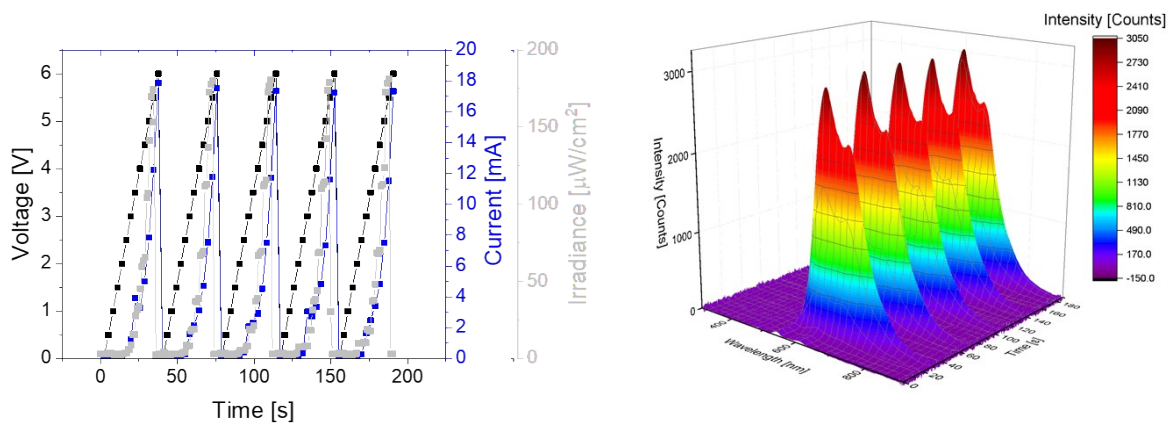


**Figure S15.** Voltage, current and irradiance profiles (left) and electroluminescent spectra (right) of **1** devices under repetitive LIV scans.

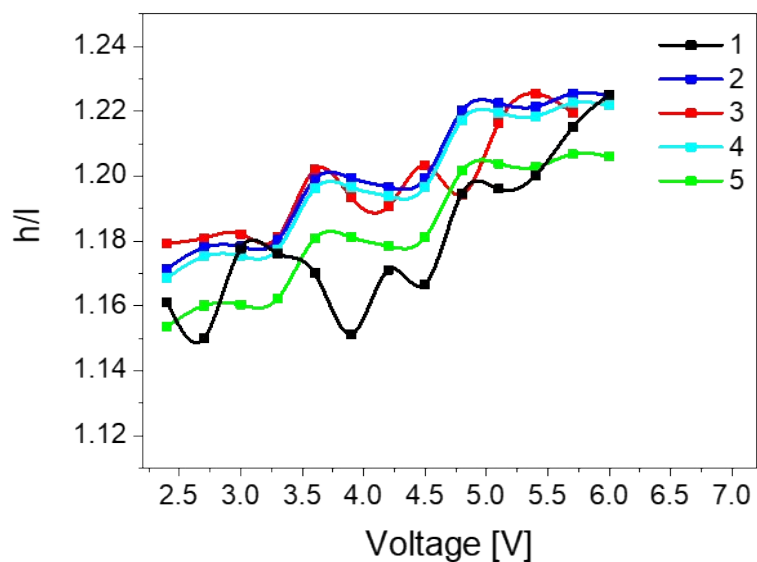


**Figure S16.**  $h/l$  ( $h$ =high energy peak and  $l$ =low energy peak) changes over applied voltage ramp upon different L-I-V (300 mV/s, 0-6 V) scans (see legend).

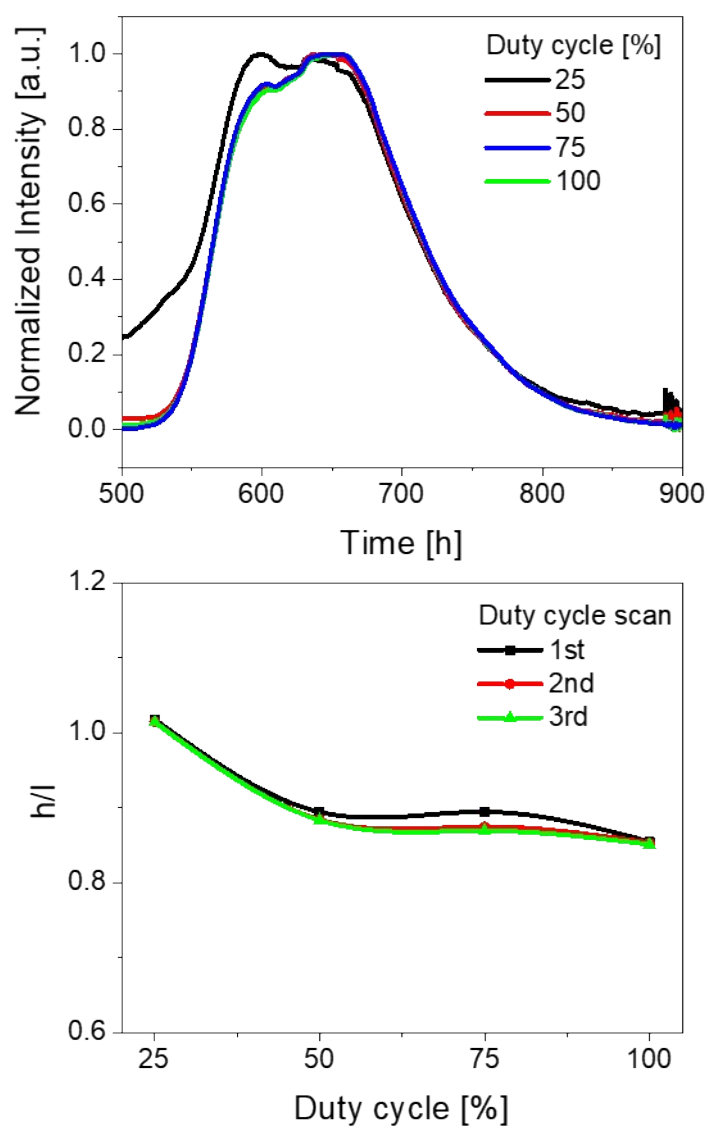


**Figure S17.** Electroluminescence response at different duty cycles (see legend) and h/l (h=high energy peak and l=low energy peak) ratio upon different duty cycle scans (see legend).

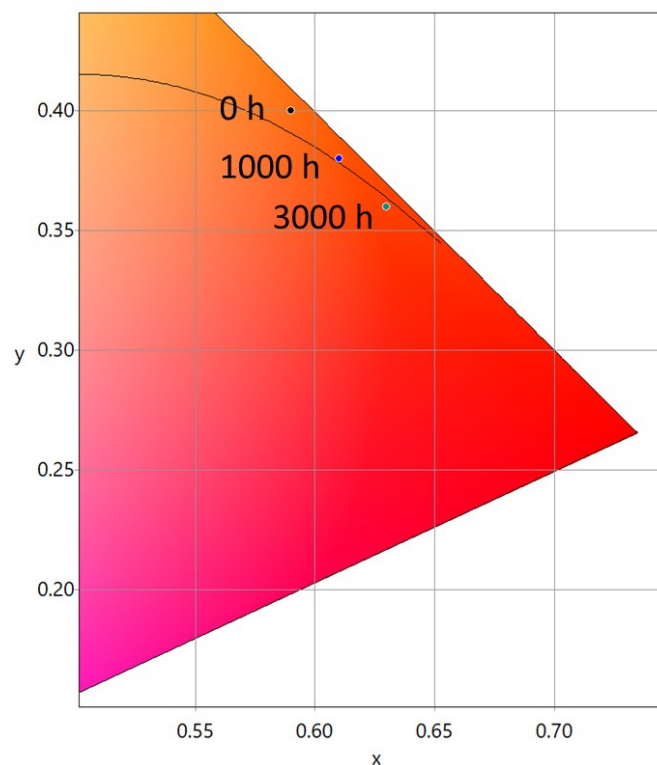


**Figure S18.** Changes of the x/y CIE coordinates of **1** devices corresponding to the electroluminescence response of fresh (black), after 1000 h (blue), and after 3000 h (green) at a pulsed 25 mA current.

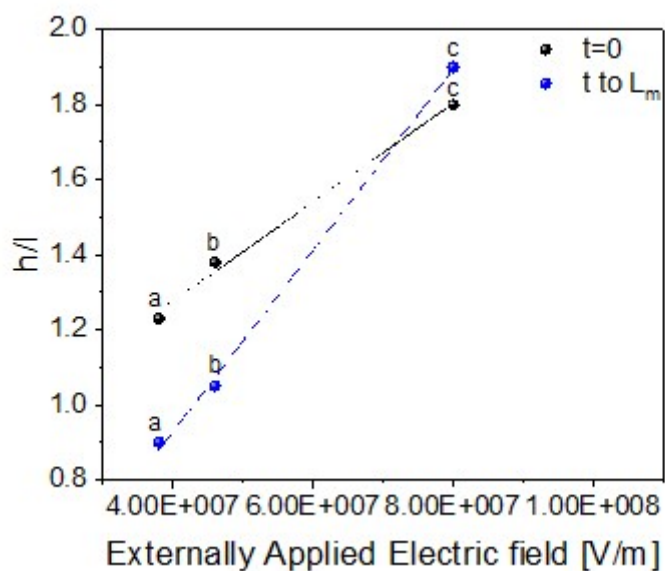


**Figure S19.** h/l (h=high energy peak and l=low energy peak) ratio vs. external applied electric field at time 0 and time needed to reach the maximum luminance ( $L_m$ ) of thick devices driven at pulsed 25 mA current (a), thick devices driven at pulsed 50 mA current (b), and thin devices driven at pulsed 25 current (c). The linear fittings ( $R^2= 0.9999$ ) are highlighted in dashed lines.

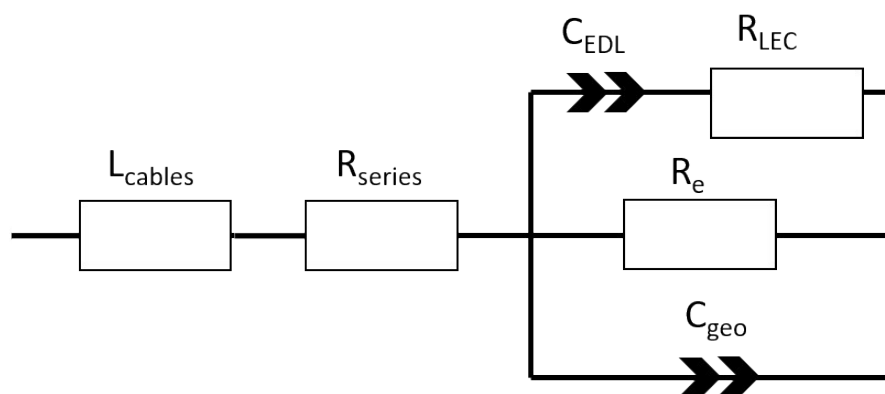


**Figure S20.** Circuit model with EDL related capacitance ( $C_{\text{EDL}}$ ), ionic resistance ( $R_{\text{LEC}}$ ), electrical resistance ( $R_e$ ), and geometric capacitance ( $C_{\text{geo}}$ ) used for dynamic EIS assays.

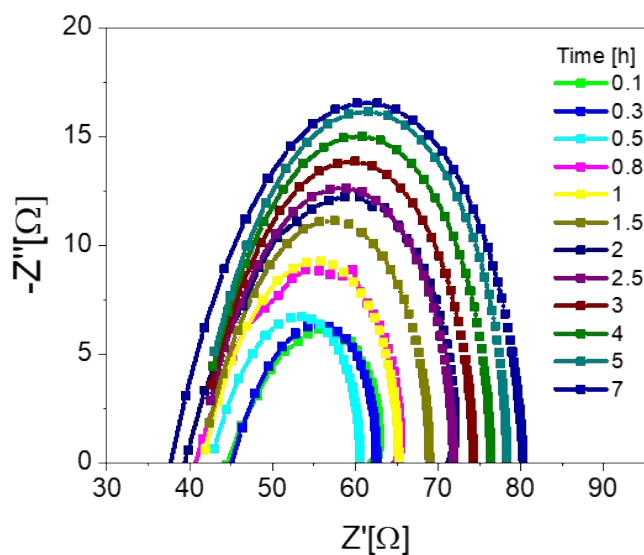


**Figure S21.** Nyquist plots of **1** devices measured under dynamic EIS at 3 V upon time (see legend). The fittings are shown in solid lines.

**Table S1. Data obtained from dynamic EIS performed at 3 V.**

Time [h]	Electrical field [V]	Doped region width [nm]	$R_{LEC}$ [ $\Omega$ ]	$C_{eff}$ [F]	$\epsilon_r$
0	1.08E+08	27.5	86.8	8.35E-09	4.4
0.15	8.69E+07	33.4	26.9	8.83E-09	4.7
0.41	7.8E+07	38.1	25.9	8.86E-09	4.7
0.58	1.04E+08	30.3	31.9	8.75E-09	4.6
1.35	1.17E+08	26.0	35.6	8.60E-09	4.6
2.1	1.34E+08	23.2	39.1	8.55E-09	4.6
3.5	2.58E+08	11.9	57.9	8.46E-09	4.5
4.4	2.61E+08	11.7	59.5	8.45E-09	4.5
7.0	3.96E+08	7.7	71.9	8.36E-09	4.4

**Table S2. State-of-art overview of red-emitting LECs.**

Type of emitter	LEC structure	Driving mode <sup>a</sup>	$L_{\max}$ (cd/m <sup>2</sup> ) <sup>b</sup> [ $\lambda_{\max}$ (nm)]	Turn-on time (h) <sup>c</sup>	Lifetime (h) <sup>d</sup>	Efficacy (cd/A)	EQE (%)	x/y CIE	Ref.
SM 1	ITO/PEDOT:PSS(70 nm)/1:TMPE:LiOTf 1:0.15:0.05(70 nm)/Al(90 nm)	25 mA <sup>a</sup>	242	24	204	-	0.78	0.61/0.39	This work
Ir-iTMC 2	ITO/PEDOT:PSS (80 nm)/Ir-iTMC: [BMIM][PF <sub>6</sub> ] 4:1 molar ratio(100 nm)/Al (70 nm)	100 A/m <sup>2</sup> <sup>a</sup>	200 [642]	870	>6000	2.0	2.0	0.63/0.37	<sup>3</sup>
Ir-iTMC 3	ITO/PEDOT:PSS (40 nm)/Ir-iTMC: [BMIM][PF <sub>6</sub> ] 80:20 wt%/Ag	2.2 V	9 [663]	-	-	3.4	7.4	0.69/0.31	<sup>4</sup>
Ir-iTMC 4	ITO/PEDOT:PSS (80 nm)/Ir-iTMC: [BMIM][PF <sub>6</sub> ] 4:1 molar ratio(100 nm)/Al (70 nm)	700 A/m <sup>2</sup> <sup>a</sup>	85 [654]	-	220	-	0.16	0.63/0.35	<sup>5</sup>
Ru-iTMC 5	ITO/Ru-iTMC /Ga:In	7.7 V	742 [690]	87 s	0.2	-	0.68 (5.9 V)	0.63/0.30	<sup>6</sup>
Ru-iTMC 6	ITO/Ru-iTMC /Ga:In	6 V	2250 [685]	-	-	0.39	0.61	0.66/0.32	<sup>7</sup>
Cu-iTMC 7	ITO/PEDOT:PSS (80 nm)/Cu-iTMC (120 nm)/Al (70 nm)	15 mA <sup>a</sup>	100 $\mu$ W/cm <sup>2</sup> [673]	-	20.9	-	-	0.66/0.32	<sup>8</sup>
ZnTPP 8	ITO/PEDOT:PSS (80 nm)/ZnTPP: TMPE:LiOTf 1:0.15:0.06 (60 nm)/Al (90 nm)	7.5 mA <sup>a</sup>	~1 [650]	20	>250	0.001	-	0.65/0.32	<sup>9</sup>
SM 9,10	ITO/PEDOT:PSS/SM 7,8 100:0.1 /Al	100 A m <sup>2a</sup>	0.6 W/m <sup>2</sup> [706]	0.1	>100	-	0.44	-	<sup>10</sup>
SM 11	ITO/PEDOT:PSS (80 nm)/SM 9: TMPE:LiOTf 1:0.10:0.06/Al (90 nm)	7.7 mA <sup>a</sup>	750 [618]	-	15	1.1	-	-	<sup>11</sup>
Red QDs	ITO/PEDOT:PSS (35	2.0	581 [620]	-	-	1.5	-	0.67/0.33	<sup>12</sup>

---

nm)/Red QDs:

[BMIM][PF<sub>6</sub>]:PVK<sup>f</sup> (150-  
200 nm)/Al

---

- a. Constant mode. b. Highest luminance achieved during the entire measurement. c. Time to reach the highest luminance. d. Time to decay to ½ of the maximum luminance. e. [BMIM][PF<sub>6</sub>]: buthyl methyl imidazolium hexafluorophosphate. f. PVK: Poly (9-vinylcarbazole).

1: Hexabenzoovalene in this work

2: [Ir(ppy)<sub>2</sub>(N<sup>^</sup>N)][PF<sub>6</sub>], with ppy=phenylpyridine, N<sup>^</sup>N=2-(6-phenylpyridin-2-yl)benzo[d]thiazole

3: [Ir(C<sup>^</sup>N)<sub>2</sub>(N<sup>^</sup>N)][PF<sub>6</sub>], with C<sup>^</sup>N=1-(4-(tert-butyl)phenyl)-1H-pyrazole, N<sup>^</sup>N=2, 2'-biquinoline

4: [Ir(C<sup>^</sup>N)<sub>2</sub>(N<sup>^</sup>N)][PF<sub>6</sub>]. With C<sup>^</sup>N=1-phenylisoquinoline, N<sup>^</sup>N= 2-(pyridine-2-yl)benzo[d]thiazole

5: [Ru<sub>2</sub>(4,4'-dimethylbpy)<sub>2</sub>(bathophen)][ClO<sub>4</sub>]<sub>4</sub>, with dimethylbpy: dimethylbipyridine, bathophen: 4,7-Diphenyl-1,10-phenanthroline

6: [Ru(hpbpip)(4,4'-dimethylbpy)<sub>2</sub>](ClO<sub>4</sub>)<sub>2</sub>, with hpbpip 2-(2-hydroxyphenyl)-1-(4-bromophenyl)-1*h*-imidazo[4,5-*f*][1,10]phenanthroline

7: [Cu(N<sup>^</sup>N)(P<sup>^</sup>P)]<sup>+</sup>, with N<sup>^</sup>N is 4,4'-diethylester-2,2'-biquinoline (dcbq) and P<sup>^</sup>P is 4,5-bis(diphenylphosphino)-9,9-dimethylxanthene (Xantphos)

8: ZnTPP Zinc-tetraphenylporphyrin

9: 1-ethyl-2-[3-(1-ethyl-1,3-dihydro-3,3-dimethyl-2H-indol-2-ylidene)-propenyl]-3,3-dimethyl-3H-indolium hexafluorophosphate

10: 1-butyl-2-[5-(1-butyl-1,3-dihydro-3,3-dimethyl-2H-indol-2-ylidene)-penta-1,3-dienyl]-3,3-dimethyl-3H-indolium hexafluorophosphate

11: 4,7-bis(4-(4-sec-butoxyphenyl)-5-(3,5-di(1-naphthyl)phenyl)thiophen-2-yl)-2,1,3-benzothiadiazole

## References

- 1 K. Baumgärtner, A. L. Meza Chinchá, A. Dreuw, F. Rominger and M. Mastalerz, *Angew. Chem. Int. Ed.*, 2016, **55**, 15594–15598.
- 2 K. Baumgärtner, F. Rominger and M. Mastalerz, *Chem. - A Eur. J.*, 2018, **24**, 8751–8755.
- 3 C. D. Ertl, C. Momblona, A. Pertegás, J. M. Junquera-Hernández, M. G. La-Placa, A. Prescimone, E. Ortí, C. E. Housecroft, E. C. Constable and H. J. Bolink, *J. Am. Chem. Soc.*, 2017, **139**, 3237–3248.
- 4 G. X. Yu, C. H. Lin, Y. X. Liu, R. H. Yi, G. Y. Chen, C. W. Lu and H. C. Su, *Chem. - A Eur. J.*, 2019, 13748–13758.
- 5 C. Momblona, C. D. Ertl, A. Pertegás, J. M. Junquera-Hernández, H. J. Bolink, E. C. Constable, M. Sessolo, E. Ortí and C. E. Housecroft, *J. Mater. Chem. C*, 2018, **6**, 12679–12688.
- 6 B. Nemati Bideh and H. Shahroosvand, *Sci. Rep.*, 2017, **7**, 15739.
- 7 B. Nemati Bideh, C. Roldán-Carmona, H. Shahroosvand and M. K. Nazeeruddin, *Dalt. Trans.*, 2016, **45**, 7195–7199.
- 8 E. Fresta, M. D. Weber, J. Fernández-Cestau and R. D. Costa, *Adv. Opt. Mater.*, 2019, DOI: 10.1002/adom.201900830.
- 9 K. T. Weber, K. Karikis, M. D. Weber, P. B. Coto, A. Charisiadis, D. Charitaki, G.

- Charalambidis, P. Angaridis, A. G. Coutsolelos and R. D. Costa, *Dalt. Trans.*, 2016, **45**, 13284–13288.
- 10 S. Jenatsch, L. Wang, N. Leclaire, E. Hack, R. Steim, S. B. Anantharaman, J. Heier, B. Ruhstaller, L. Penninck, F. Nüesch and R. Hany, *Org. Electron.*, 2017, **48**, 77–84.
- 11 S. Tang, W.-Y. Tan, X.-H. Zhu and L. Edman, *Chem. Commun.*, 2013, **49**, 4926–4928.
- 12 G. Qian, Y. Lin, G. Wantz, A. R. Davis, K. R. Carter and J. J. Watkins, *Adv. Funct. Mater.*, 2014, **24**, 4484–4490.